Formulas for Fabry-Perot Velocimeter Performance Using Both the Stripe and Multifrequency Techniques
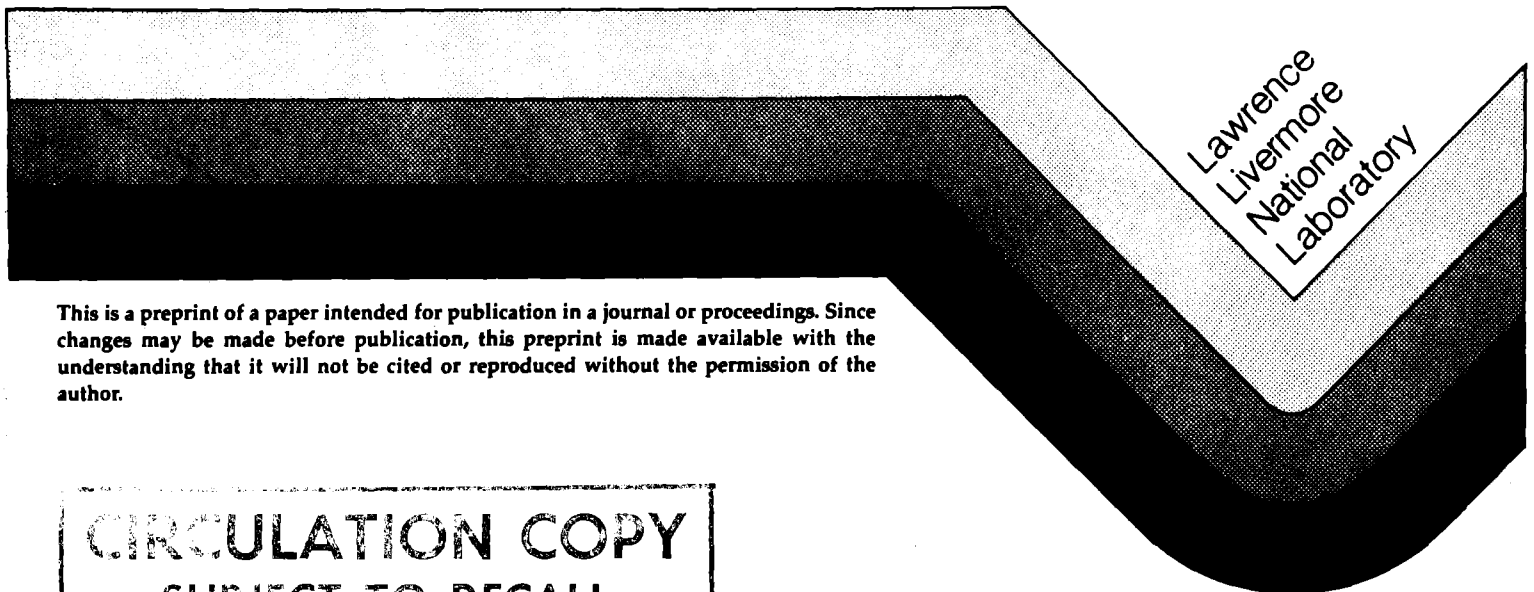
D. R. Goosman

July 13, 1989

Lawrence Livermore National Laboratory

DISCLAIMER

Formulas for Fabry-Perot Velocimeter Performance Using Both the Stripe and Multifrequency Techniques

David R. Goosman
Lawrence Livermore National Laboratory
P.O. Box 808, Livermore, CA 94550

Abstract

New stripe and multifrequency techniques for Fabry-Perot velocimetry are incorporated into an analytical model for the entire system. Properties of striped Fabry-Perot (FP) interferometers are derived. An understanding of energy flow in both striped and unstriped FPs is presented. Nine contributions to the velocity resolution are examined and analytical approximations provided for each of them. Formulas for the overall velocity and time resolution of each fringe are derived. Using brightness arguments to put limits on the maximum usable light acceptable by the system, we have also derived analytical limits on the photographic writing speed of each fringe.

I. Introduction

Optical velocimetry based on Fabry-Perot (FP) interferometers operating in the fringe mode is a widely used measuring technique in research with explosives, gas-propelled projectiles, and electrically accelerated objects.[1] Since Ref. 1 was published, two recent new ideas providing more capability for this technique have emerged. Gidon and Behar[2] have demonstrated an order of magnitude more laser power by using a pulsed dye laser followed by an FP filter set to the same spacing as the conventional analyzer FP. The interference patterns for each filtered frequency overlap almost perfectly at the slit of the streaking camera, effectively making all of the nonmonochromatic filtered power useful. In addition, McMillan et al.[3] have applied a striped analyzer FP to use more efficiently the light reflected by a moving test object. In this technique, one removes a narrow stripe of the reflective coating on the upstream mirror in order to avoid the large losses (of the order of 90%) that normally arise from reflection.

These two ideas are not without some drawbacks, however. The multifrequency technique involves a slight broadening of most of the interference fringes due to the imperfect overlap, and the stripe technique involves the problem of getting the reflected light to enter the stripe. The latter issue is a function of the size of the illumination on the target, averaged over the target travel distance, and the solid angle of the collection optics.

Our purpose in this paper is to provide a set of fairly simple analytical formulas for users to compare the total velocity resolution, time resolution, and photographic writing speed of one striped velocimeter configuration with another. The major simplification in our approach is the treatment of the fraction of light reflected by the target that can enter the instrument. We have written a code, called STRIPE, that calculates in detail the amount of light at each instant of time from a moving Lambertian target that enters an array of real collection fibers and how that light exits the fibers and illuminates the stripe on the FP mirrors. To present the results as analytical formulas, however, we do not use the STRIPE code here.

Instead, we simply calculate the ratio of the emittance (or brightness) acceptance of the instrument to the emittance reflected by the target. This helps to determine, for any optical transport system between the target and the instrument, an upper limit on the amount of useful light. Work with the STRIPE code has shown us that it is not difficult for real systems to collect 30% of the amount of light represented by the emittance-argument limit. The present work is intended to be useful in comparing various

reflectivities, mirror spacings, and streaking-camera properties to see how they affect the net time and velocity resolutions and the upper limit on the photographic writing speed for each interference fringe.

We derive a simple analytical result for the effect on fringe finesse of the angular divergence of light entering an FP filter. We also derive several properties of striped FPs. For example, we present a good simple analytical approximation for the total finesse of a striped FP with finite-sized, nonflat mirrors. An explanation of some of the properties of normal as well as striped FPs with regard to energy flow is given. It is shown below that diffraction plays a key role in understanding energy transport in the striped FP, even for light beams several centimeters in diameter. Figure 1 shows the system being modeled. A dye-pumped laser oscillator beam[2] is expanded by a telescope to reduce angular divergence. It then enters an FP filter, is transported to the target, reflected, and collected by a lens. This light is then converged in one dimension by a cylinder lens and enters an analyzer FP with a stripe of its reflective coating removed. The exiting light is focused by a spherical lens onto the slit of an electronic streaking camera.

II. Properties of Normal and Striped Interferometers

A. The Striped FP Interferometer

Figure 2 shows the striped FP interferometer. The upstream mirror of intensity reflectivity R_1 has a stripe of half-width R_{st} removed. The length of the stripe equals the mirror diameter. The entire downstream mirror is coated with reflectivity R_2. We first consider only light incident at a large enough angle that multiple reflection occurs, as indicated in Fig. 2. It is straightforward, using the standard formalism illustrated for normal FPs in Born and Wolf,[4] to calculate the intensity at the focal plane of a spherical lens vs incident angle for perfectly flat mirrors. The sum of the transmitted beamlet amplitudes is

$$A_T = \frac{t_2}{1 - r_1 r_2 e^{i\delta}} \quad ,$$

(1)

where the phase δ is given by

$$\delta = \frac{4 \pi h \, v \cos \theta}{c}$$

(2)

and h is the mirror separation, v is the frequency, and c is the speed of light. Here r_1 and r_2 are the amplitude reflectivities of the two dielectric coatings, and t_2 is the amplitude transmission of the second coating. The ratio of transmitted to incident intensities is

$$I_s = \frac{T_2}{(1 - R)^2} \frac{1}{1 + \dfrac{4 R \sin^2 \delta/2}{(1 - R)^2}} \quad ,$$

(3)

where the reflectivity R is given by

$$R = \sqrt{R_1 R_2}$$

(4)

and

$$T_2 = |t_2|^2 = 1 - R_2 - A = 1 - |r_2|^2 - A \quad .$$

(5)

The coefficient A is typically about 0.002 and accounts for absorption and scattering in the second mirror. Peaks in the transmission occur when the phase is a multiple of 2π. In the present paper, these

2

peaks will be due to variations in either frequency or angle. If we set $R_1 = R_2 = R$ in Eqs. (4) and (5), then Eq. (3) agrees with an expression (5.3.1) given in the text by Hernandez[5] for a side-illuminated FP. A striped FP allows one to see fringes on both sides of the center of the pattern, as opposed to the side-illuminated FP. As pointed out in Ref. 1, the analysis of the pattern is much easier if fringes on both sides of 0 deg are available.

The resonant angles θ_j of Eq. (3) are[6]

$$\theta_j = \cos^{-1}\left\{\frac{\lambda}{2h}\left[INT\left(\frac{2h}{\lambda}\right) - K + 1\right]\right\} \doteq \sqrt{\frac{j\lambda}{h}} , \qquad (6)$$

where INT means the integer part of, λ is the wavelength, k is a positive integer (usually less than 5), and j is given by

$$j = k - 1 + \epsilon = k - 1 + \frac{2h}{\lambda} - INT\left(\frac{2h}{\lambda}\right) . \qquad (7)$$

Here ϵ is the fractional order of interference and has a value between 0 and 1. The index j is a real number. This notation is shown in Fig. 3. Our $k - 1$ is the j of Ref. 1. The second form of Eq. (6) is a very good approximation to the resonant angles, since they are usually smaller than 0.01 rad.

The ratio of the separation of the transmission peaks to their full width at half-maximum, when the phase, or the product $v \cos \theta$, is varied, is called the finesse, and is given by

$$\mathcal{F} = \frac{\pi}{2 \sin^{-1}\left(\dfrac{1 - R}{2\sqrt{R}}\right)} \doteq \frac{\pi\sqrt{R}}{1 - R} , \qquad (8)$$

the latter form being the limit for large R, which is accurate to 0.1% for R greater than 0.86.

If $R_1 = 1$, then the transmission of the striped FP can be written

$$I_s = \left(1 - \frac{A}{1 - R^2}\right)\frac{1 + R}{1 - R}\frac{1}{1 + \dfrac{4 R \sin^2 \delta/2}{(1 - R)^2}} . \qquad (9)$$

For a given finesse, and thus for a given value of R, it will often be best to have $R_1 = 1$, since this produces about twice the peak intensity compared to having $R_1 = R_2 = R$. For example, Eqs. (3) and (9) show that a pair of 99.8% and 92.3% reflectivity mirrors with $A = 0.002$ transmit about 1.95 times as much light as a pair of 96% mirrors, but both have the same finesse or velocity resolution. The reason is that with $R_1 = 1$, almost all of the energy must exit to the right of the mirror pair. The advantage in doing this was not recognized in Ref. 3.

An advantage of the stripe over the normal FP is shown by comparing Eq. (9) with the result[4,5] for the normal FP:

$$I = \left(1 - \frac{A}{1 - R}\right)^2 \frac{1}{1 + \dfrac{4 R \sin^2 \delta/2}{(1 - R)^2}} , \qquad (10)$$

where R is the reflectivity common to both mirrors. For incident light that enters the stripe, when $R_1 = 0.998$, $R_2 = 0.923$, and $A = 0.002$ the peak intensity for the striped FP is 51 times as large as that for the normal FP with $R = 0.96$ and the same finesse. In most cases, part of this transmission advantage is cancelled out because only a fraction of the illumination can be made to enter the stripe. The stripe technique will be advantageous when the product of the illumination size on the target and the angular range of the collected light is small enough. Comparing Eqs. (9) and (10) shows that the absorption A decreases the peak transmission of the normal FP by a larger percentage than it does for the striped FP with $R_1 = 1$. For $A = 0.002$ and $R = 0.97$,

3

absorption decreases the normal FP peak transmission by 13% but drops the striped FP transmission by less than 4%. This can be understood qualitatively by considering just a single beam traversing the first mirror of the normal FP. Then absorption makes the first transmitted intensity = 0.028, rather than 0.030, for a 7% loss in output.

The averages over phase from 0 to 2π—that is, over one free spectral range—are important for the discussions below. They are

$$\frac{1}{2\pi} \int_0^{2\pi} I_s \, d\delta = 1 - \frac{A}{1 - R^2} \tag{11}$$

for the striped FP with $R_1 = 1$ and

$$\frac{1}{2\pi} \int_0^{2\pi} I \, d\delta = \left(1 - \frac{A}{1 - R}\right)^2 \frac{1 - R}{1 + R} \tag{12}$$

for the normal FP pattern.

B. Equal Reflectivity Mirrors for the Striped FP

Another mode of operation for the striped FP is to use equal reflectivity mirrors. One can compensate for the factor of two in peak transmission mentioned just after Eq. (9) for the light that enters the stripe by using some of the light that cannot enter the stripe. We normally set the angular divergence approaching the stripe to just cover four transmission peaks. Suppose that under this constraint the illumination cannot be made smaller than 25 times as large as the stripe. Then, for the example above for R = 0.96, the transmitted intensity is about the same regardless of whether or not $R_1 = 1$. One problem with this mode of operation, however, is that if any light missing the stripe is converging towards the optical axis, some of the multiply reflected beams may eventually exit back through the stripe. This creates a fringe broadening due to the limited number of beamlets created. For example, if the full width of the stripe were 0.7 mm, and the illumination 18 mm wide (so that the intensity would be equivalent), the mirrors would effectively be only 9 mm in radius for such rays.

For 9-mm-radius mirrors with h = 6.5 cm and R = 0.96, Section IV.E below on walkoff broadening allows one to calculate that, for these special rays, the finesse is degraded from 76 to 17 due to walkoff.

One might try to set up the illumination at the stripe so that the light diverges away from the optical axis, and reflection back through the stripe cannot occur. This could be ensured by using fiber-optic transport between the reflecting target and the optics just preceding the stripe. Thus, when the reflecting target moves, the light entering the stripe would not change from divergence to convergence, as it could for an air-transport system.

To ensure divergence, one would set the waist of the illumination upstream of the stripe. The rays at the waist of spatially incoherent illumination usually have an angular distribution that is not significantly correlated with the radius of the ray. It is easy to show that the illumination at the stripe must be at least twice the diameter of the waist to completely eliminate convergence.

Unfortunately, the angles of the rays entering the first mirror would then have a correlation with position, with the large radii corresponding to large angles. If the illumination has a radius of 9 mm to match the transmitted power of an FP with $R_1 = 1$, then the outer rays hitting a 25-mm-radius mirror walk less distance before vignetting. Thus they would have a larger walkoff broadening than would an FP with $R_1 = 1$. Thus, unless the mirrors are large enough, attempting to get more power transmission by using equal reflectivity mirrors would necessitate broader fringes.

There is one situation with an equal reflectivity FP that should be avoided experimentally. Suppose the position of the illumination waist near the stripe is allowed to move during the dynamic experiment, as would happen with an air-transport system. The system's velocity resolution would be tested with a static target (static waist position) for which we assume that all the rays diverge into the FP. Then, if the waist size is only a few millimeters, the walkoff broadening is minimal and the fringe sharpness would appear to be good. During the dynamic motion of the target, however, the position of the waist may move

4

towards the striped FP and allow converging rays to enter the nonstriped region. Then reflections back through the stripe will occur and make the fringes significantly broader than they were compared with the initial test.

In summary, if the mirrors are large enough there may be situations where more intensity at no loss of velocity resolution results from using equal reflectivities. But for our applications this is unlikely, because it is usually possible to make the waist radius only a few millimeters. Also, if the waist is this small, no significant broadening will occur with equal reflectivities if divergence of the rays is ensured, but more transmitted power would result from using $R_1 = 1$.

C. Energy Flow in the Striped FP Interferometer

When looking at Fig. 2, the reader might wonder how energy can be conserved in this system. Consider for example, lossless mirrors with $A = 0$ and $R_1 = 1$. Consider also only light entering with a large enough angle that it misses the stripe after the first reflection, as indicated for the rays shown in Fig. 2. Clearly all of the incident energy must end up to the right of the second mirror. However, if the angle is chosen to correspond to mid-resonance, where the sine term in Eq. (9) equals unity, then Eq. (9) gives

$$I_s = \frac{1 - R}{1 + R} \tag{13}$$

for the transmission at the focal plane of a lens to the right of the FP. This quantity is much less than unity. What happened to the rest of the energy? The answer to this involves diffraction.

One can first use approximate arguments to see what happens. Consider a spatially coherent, azimuthally symmetric Gaussian laser beam with a waist located at the stripe, as in Fig. 4. If most of the beam energy is to enter the stripe, the beam must have a waist radius R_0 (the e^{-2} intensity radius) less than or equal to R_{st}. The beam centroid angle is θ_j with respect to the normal to the mirrors. If most of the beam is to multiply reflect, we must have

$$h\,\theta_j > R_{st} \quad . \tag{14}$$

But the half-angular spread θ_b of the beam due to diffraction (or just the nature of the Gaussian beam) will be

$$\theta_b \doteq \frac{\lambda}{\pi R_0} \geqq \frac{\lambda}{\pi R_{st}} > \frac{\lambda}{\pi h\,\theta_j} = \frac{\theta_j}{j\,\pi} \quad , \tag{15}$$

the latter forms resulting from Eqs. (14) and (6). These angles will exist after the beam has traversed a distance Z_0 away from the waist equal to

$$Z_0 = \frac{\pi R_0^2}{\lambda} < \frac{\pi h^2\,\theta_j^2}{\lambda} = j\,h\,\pi \quad . \tag{16}$$

The latter equality follows from Eq. (6). Thus the angles develop after about $\pi j/2$ beamlets have formed, compared to the total number of beams needed for the FP pattern to reach 99.7% of its final intensity, which is equal to about twice the finesse. Since j will be usually less than 4, and the finesse will usually exceed 30, the angles will be developed after only 10% of the useful beamlets have been created.

Now we estimate how broad the diffraction-induced angular range is compared with a free spectral range (FSR). The latter is defined in θ^2 space by

$$FSR = \theta_{j+1}^2 - \theta_j^2 = \frac{\lambda}{h} \quad , \tag{17}$$

5

which is independent of j. The breadth in θ^2 space resulting from using Eq. (15) is

$$\left(\theta_j + \theta_b\right)^2 - \left(\theta_j - \theta_b\right)^2 = \frac{4\,\mathrm{FSR}}{\pi} \quad , \tag{18}$$

which is larger than one FSR.

Thus, these approximate arguments indicate that if most of the beam entering the stripe multiply reflects it will naturally have enough angular divergence to fill at least one complete FSR! Equation (11) indicates that the transmission of the lossless, striped FP, averaged over an FSR, is unity. Thus, diffraction ensures that energy is conserved. If a plane wave instead of a focussed Gaussian beam were incident on the stripe, then diffraction from the finite size of R_{st} will have a similar effect. The above arguments used spatially coherent light, but for spatially incoherent light the diffraction spreading would have a similar result.

One might expect diffraction to be important for striped FP systems, since the stripe will usually be smaller than 1 mm wide. However, the above arguments are independent of the size of the stripe! Even for wider stripes, diffraction will still cause an entire FSR to be filled as long as the beam centroid entrance angle is large enough for most of the light to multiply reflect. This is because that centroid angle must increase as R_{st} increases, and as the angle increases the spacing between adjacent resonant angles decreases.

Thus an important property of the striped FP is that one can never make an entire beam have a transmission given by Eqs. (3) or (9) for a unique angle (or phase). The utility of the striped FP is thus in the fringe mode and not in a scanning mode. On the contrary, an entire beam entering a normal FP can have a transmission determined by Eq. (10) evaluated for a unique angle, if its diameter is large enough.

The striped FP would therefore not be advantageous for many applications, but it is for velocimetry. Either Eq. (3) or (9) can be used to describe the transmission of each angular component of the beam. Diffraction-induced angular spreading of 1 FSR is not a problem, since we purposely introduce about 4 FSRs of angular spread with the cylinder lens. If four fringes are desired, we could set the cylinder lens to make 3.5 FSRs and count on the stripe to increase it to about four.

The arguments leading to Eq. (18) were not very rigorous. Because of this we have calculated in detail the superposition of sixty Gaussian elliptic beams at the focal plane of the spherical lens, simulating a striped FP with a finesse of 30. The beamlets were modelled by Gaussian elliptic beams due to the cylinder lens of Fig. 1. The beamlets arose from multiple reflections within a striped FP. Each beamlet, after passing through the spherical lens, crossed the focal plane at a different centroid angle, had a different waist size, waist location, amplitude, and phase. The phases were appropriate for having arisen from a single Gaussian beam entering a stripe whose width was twice the beam radius. The result is that the expected FP pattern resulted, covering about 1 FSR for a unique centroid angle of the beam entering the stripe. This agrees with the result of Eq. (18) derived above less rigorously.

D.   Energy Flow and Diffraction for the Normal FP

In the lossless normal FP, there is no constraint analogous to Eq. (14) on the entrance centroid angle. The entrance beam may be large enough that it remains essentially the same diameter throughout its many reflections. Therefore one could make a real beam to appear as shown in Fig. 5. The peak transmission at a resonant angle can be unity, provided the angular spread of the beam is small compared to the half-width of the transmission pattern given by Eq. (10). But the entire beam transmission at the focal plane of the spherical lens cannot be unity unless the total power exiting the second mirror is also unity. The latter cannot happen unless all the transmitted beamlets of Fig. 5 overlap well spatially, and it would appear at first that those beamlets need not overlap.

Again, diffraction is the answer. Assume that the diffraction-induced angular spread is small compared to the angular width of the transmission pattern [Eq. (10)] for the normal FP. Then diffraction causes the beam radius [obeying Eq. (15)] entering the normal FP to be larger than a minimum size. It is easily shown that after all the useful beamlets have formed, the transverse offset of the last beam is small compared with the original beam size and good overlap occurs. The beamlets shown in Fig. 5, which do not overlap spatially, must have a large enough angular spread to fill at least one FSR.

6

E. The FP Pattern for Illumination Filling the Stripe

Equation (3) is only part of the interference pattern due to the striped FP, however, since its derivation assumed that the light entered at such an angle that it multiply reflected from both mirrors. The finite width of real beams means some of the light will reflect back through the stripe and be lost. Consider, for example, a slightly more general beam of light, one that illuminates the entire stripe. For the moment we will still use the ray-tracing formalism. We see from Fig. 2 that if the ray entrance position x is such that

$$x > R_{st} - 2 h \tan \theta \quad , \tag{19}$$

then the light will be multiply reflected. Otherwise, it will pass through the second mirror only once before adding to the interference pattern at the focal plane of the spherical lens. To keep the problem simple, we assume that $R_1 = 1$, so that even if the illumination is larger than the stripe, only the light entering the stripe can contribute to the interference pattern. If $R_1 \neq 1$, then some of the light falling outside the stripe will pass through both mirrors.

Setting $R_1 = 1$ is the most light-efficient choice as well. In addition, we assume that the stripe area has an antireflection coating, so that $R = 0$ within the stripe. Appendix A treats the case where the stripe region has no antireflection coating.

Consider the light at a specific angle θ filling the stripe with $R_1 = 1$ in Fig. 2. The fraction that enters the stripe that is multiply reflected is given by

$$q = \min\left(1, \frac{h\,\theta}{R_{st}}\right) \quad , \tag{20}$$

and the remainder is not reflected. To calculate the interference pattern in the lens focal plane, we assume that the light is spatially incoherent.

F. Spatially Incoherent Light-Ray-Tracing Formalism

For a beam that is spatially very incoherent (the usual case for velocimetry from shock-driven surfaces), we treat the contributions from rays with different x values incoherently. Thus the intensity at the lens focal plane divided by the intensity entering the stripe is

$$I_s = T_2\left[1 - q + \frac{q}{(1-R)^2} \frac{1}{1 + \dfrac{4\,R\,\sin^2 \delta/2}{(1-R)^2}} \right] \quad , \tag{21}$$

where T_2 and q are given by Eqs. (5) and (20), respectively.

Fortunately, the contribution of the first term $(1 - q)$ is quite small compared to the peak intensity in normal circumstances. The first term in Eq. (21) is most important for small angles. For resonant angles (those for peak transmission), the ratio of the first to second terms is

$$\frac{\text{Term 1}}{\text{Term 2}} = \left(1 - R^2\right)\left(\frac{1}{q} - 1\right) \quad . \tag{22}$$

The resonant angles for the spatially incoherent result, Eq. (21), are almost exactly the same (for $R > 0.9$) as those for the normal FP. As an example of the spatially incoherent case, for $h = 6.5$ cm and $\lambda = 0.000051$ cm, the first three resonant angles are at 1.98, 3.44, and 4.44 mrad. We then evaluate the effect of the nonresonant term of Eq. (21) for the case where $R_{st} = 0.037$ cm and $R = 0.9$. The ratio, Eq. (22), is about 0.019, 0.007, and 0.003, respectively, for the three resonant angles listed above. For reflectivities higher than 0.9 for the analyzer FP, the effect is even smaller. In principle the peak angle is shifted slightly from that given by Eq. (21) due to the $h\theta$ terms of Eq. (21), but the shift is less than 0.0001 mrad for the first resonant angle in the case above. The finesse is about 3% less than for the normal FP for this case.

G. Discussion of Validity of Section II.F for Real Beams

Equation (21) used a ray-tracing formalism and incoherent addition of beam intensities from different spatial entrance positions x of Fig. 2. That derivation neglected the increased angular spread of the beam due to diffraction from the limited size of the stripe. Equation (21) is the transmission, averaged over x, for light at a particular angle. For real beams, one would then evaluate Eq. (21) over the angular distribution of light present in the beam. The latter operation is not straightforward, since the angular spread of the beam may be somewhat larger, after diffracting from the stripe opening, than it was originally. Equation (21) should be a rough approximation to the beam intensity vs angle for a spatially incoherent beam coming to a waist at the stripe provided the initial angular spread is large compared to the diffraction spreading. We normally would have an incident beam with an angular spread of four fringes and a stripe size that for that beam limits diffraction spreading to about one fringe.

The purpose of Eq. (21) is to illustrate that there is a nonresonant background beneath the resonant fringe terms for real beams and that in normal circumstances the changes in finesse and peak shifts are negligible compared to those of Eq. (3).

H. Determining the Width of the Stripe

The results above allow us to discuss a simple rule to guide the user in choosing the half-width R_{st} of the stripe. We assume that the illumination of the stripe shown in Fig. 2 has a size larger than the stripe and that the entrance position x of the ray is uncorrelated with the entrance angle θ.

Less of the small-angle light will undergo multiple reflections than does the large-angle light. Thus the inner peaks in the transmission-vs-angle plot (fringes) suffer an intensity loss compared with the outer fringes, as expressed by Eq. (21). Light with a large enough angle will multiply reflect for any entrance position x within the stripe.

We use the result for spatially incoherent light, which applies to our velocimetry measurements. Normally the cylinder lens of Fig. 1 produces an angular convergence, θ_{cyl}, large enough to produce about four resonant angles (fringes). Define the real number p_{cyl} by the relation

$$\theta_{cyl} = \sqrt{\frac{\lambda\, p_{cyl}}{h}} \quad . \tag{23}$$

Comparing Eq. (23) with Eq. (6), we see that the cylinder lens provides enough angular convergence to produce p_{cyl} resonant angles if 0 degrees is not resonant and $p_{cyl} + 1$ angles if 0 degrees is resonant (i.e., $\epsilon = 0$). Now define another real number p_{str} by the relation

$$R_{st} = \sqrt{\lambda\, h\, p_{str}} \quad . \tag{24}$$

This means that

$$q = \frac{h\,\theta_j}{R_{st}} = \sqrt{\frac{j}{p_{str}}} \tag{25}$$

if j is less than or equal to p_{str}. Here we can think of j as the fringe number being considered and p_{str} any number smaller or equal to p_{cyl}, which is the maximum fringe number. The resonant second term of Eq. (21) describes fringes whose peak intensities increase as the square root of the fringe number j, until j reaches p_{str}.

Our goal is to provide formulas that will allow the entire velocimetry system to be approximately optimized. However, a simple guide to choosing R_{st} can be made by first assuming that the illumination at the stripe is fixed and larger than the stripe. Then it is clear from Eq. (21) that increasing R_{st} beyond $\sqrt{j\lambda h}$ does not increase the intensity of the jth fringe. This is because only the light at angle θ that enters the stripe within a distance $h\theta$ will be multiply reflected. A good choice for determining the value of R_{st}, as first suggested by McMillan,[7] is to set $p_{str} = p_{cyl} = 4$. Then a j = 1 fringe (if resonant) would have half the

peak intensity of the $j = 4$ fringe. For a fixed illumination size, increasing R_{st} beyond this value does not increase fringe brightness, and in fact decreases fringe contrast, due to the increased contribution of the first term in Eq. (21).

I. Changing the Illumination Size

What if both R_{st} and the illumination size are changed but the angular range determined by p_{cyl} is kept fixed? Consider doubling both R_{st} and the size of the illumination. As will be explained below, this may allow double the target light to be collected and to enter the larger stripe within the same angular range. However, it also causes a reduction in the fraction of light entering the larger stripe that gets multiply reflected. No net gain is achieved. This is because only the light entering within a fixed distance from the edge of the stripe can contribute to the first fringe.

What if we change just the illumination size and p_{cyl}? Suppose we started with R_{st} set by using $p_{str} = 4$ and an illumination angular range that covers four fringes ($p_{cyl} = 4$) and is spatially much larger than R_{st}. We may then use a stronger cylinder lens to decrease the illumination to a size just larger than R_{st}. This increases the angular range, however, and the light per unit angle per unit distance x (Fig. 2) does not change, so the fringe intensity stays the same. What is gained by this stronger focusing, however, is that the streaking camera can be much closer to the analyzer FP, reducing the length of the entire system by meters in some cases.

III. Properties of the Source

A. The Oscillator and Telescope

The source shown in Fig. 1 is a laser amplifier designed by Steinmetz[1] and converted to an oscillator by means of external mirrors. Define the time-integrated bandwidth to be Δv, the center wavelength to be λ_0, the time-averaged divergence to be θ_0, the beam radius to be R_0, and the optical path between mirrors to be h_0. Steinmetz's oscillator has $\Delta v = 2.3 \times 10^{12}$ Hz, so that $\Delta\lambda = 20$ Å, $\lambda_0 = 5100$ Å, θ_0 equal to about 0.9 mrad, R_0 roughly equal to 0.2 cm, and $h_0 = 50$ cm.

An expanding telescope just upsteam of the filter FP reduces the angular divergence of the oscillator to minimize the broadening of the analyzer FP fringe pattern. If the telescope magnification is M, then the maximum output angle is θ_0/M.

Figure 6(a) shows a part of the distribution of oscillator output power per unit frequency vs frequency. This frequency distribution is assumed to be independent of the angle of the light exiting the oscillator. The width of the individual oscillator modes is denoted by W_0. Also shown in Figs. 6(b) and (c) are filter transmission curves for two angles for $h = 6.5$ cm and $R_f = 0.91$. The transmission curve for the nonzero angle has peaks that lie at slightly higher frequencies than their 0-deg counterparts. The nonzero-angle transmission peak frequency $v_{1(\theta)}$ and v_{10} as defined in Fig. 6, are related by

$$v_1(\theta) = \frac{v_{10}}{\cos\theta} \quad , \tag{26}$$

and the mode separation is given by

$$v_2(\theta) - v_1(\theta) = \frac{c}{2\,h_f\cos\theta} \quad , \tag{27}$$

where v_2 and v_1 are adjacent mode peak frequencies as shown in Fig. 6, and h_f is the mirror spacing of the filter.

9

The peak frequencies of the filtered spectrum, after reflecting from a target and analysed by the analyzer FP, will make fringe patterns that almost overlap if $h_f = h_a$. The broadening due to this imperfect overlap vs fringe number, called the overlap broadening, was introduced in Ref. 2 and treated in detail in Ref. 6. It is the broadening that would still exist for large filter and analyzer finesses and for negligible angular divergence entering the filter.

B. Population of the Modes

An oscillator frequency ν_m that overlaps any resonant part of the filter transmission pattern of Fig. 6 will be fairly efficiently transmitted. Only some of the filter modes will be populated by an oscillator mode, depending upon the actual values of mode separations and mode widths. The ratio of mirror spacings h_0 and h_f is intended to be random and not equal to the ratio of two small integers. Fewer than 1000 filter mode peaks [regions within one half-width, half-maximum (HWHM) of a peak in the transmission pattern] could be populated for the example of Fig. 6, and the probable number is less. For the worst case of very narrow oscillator modes, the probable number is about 8000 divided by the finesse of the filter, or about 240 for $R_f = 0.91$.

However, since the transmission pattern is repetitive, we may examine the population of possible transmissions by evaluating each oscillator frequency modulo the mode separation $c/[2h \cos (\theta)]$ of the filter. This produces 8000 sampling points within one FSR of the filter, and about 240 within one HWHM of the peak. Thus, it is reasonable to assume that the entire transmission pattern spanning one FSR of the filter FP is normally well-sampled by a near-continuum of available oscillator frequencies (modulo the filter mode separation).

If the oscillator spectrum bandwidth at a given time is very narrow (less than a few Å) and the center wavelength changes with time (slewing), then the statistical sampling must be verified more quantitatively. We have shown with a Monte Carlo calculation (picking h_0 at random) that if the instantaneous bandwith of the oscillator is greater than about 4 Å, the oscillator mentioned above will sample well the transmission pattern of a filter with $h_f = 6.5$ cm with $R_f = 0.91$, even if the modes of the oscillator are very narrow. A finite width of the oscillator modes makes the smoothness of the sampling even better.

We also assume that the angular distribution of the oscillator output is constant per unit solid angle out to an angle θ_0 and that this distribution is the same for all frequency components.

C. Power Transmission Integrated Over Angle

Under these conditions, we can infer the ratio of angle-integrated power exiting the filter to that entering. Consider the light of a specific frequency entering the filter within a range of θ^2 that is narrow compared to the half-width in θ^2 space of a transmission peak. That is,

$$\Delta(\theta^2) < \frac{\lambda}{2\,h_f\,\mathscr{F}_{\text{filt}}} \quad , \tag{28}$$

where $\mathscr{F}_{\text{filt}}$ is the finesse of the filter. In view of the arguments given above, it is clear that for the light in this narrow angular range, the transmission curve is well sampled over frequency and averages to the result of Eq. (12). But this same argument holds for any narrow angular range, and hence for all angles. Thus the expected power transmission integrated over angle is

$$\frac{P_{\text{out}}}{P_{\text{in}}} = \frac{1 - R_f}{1 + R_f} \left(1 - \frac{A}{1 - R_f}\right)^2 \quad . \tag{29}$$

This result is independent of the angular divergence of the light, as long as the ratio of h_0 to $h_f \cos (\theta)$ is not a simple rational number for any angle entering the filter. Normally the divergence entering the filter is very small, of the order of 0.2 mrad, and $1 - \cos 0.0002 = 2 \times 10^{-8}$, so that the above criterion would normally be valid for all angles in the beam.

10

However, if the divergence is very large, of the order of 140 mrad (which would not be the case for our application), then $1 - \cos(\theta) = 0.01$, and it is fairly likely that some angles will be transmitted with significantly different efficiency from others. Even though the ratio may obey the above criterion at 0 deg, it has a good chance of violating it for some other angle θ_x within a beam of such large divergence. Then the transmitted power for light at angle θ_x can differ radically from the value given by Eq. (29). If the modes align with peaks in the transmission spectrum, the power will be higher than Eq. (29). If they synchronize at transmission minimima, then the power will be less than Eq. (29).

IV. Velocity Resolution of the Entire System

Several factors affect the velocity resolution for the configuration shown in Fig. 1. We estimate these factors as the first step in putting together a set of formulas for comparing the velocity and time resolution and photographic writing speed between specific configurations.

A. The Filter

The filter broadens the analyzer FP fringe pattern for two reasons. The first is the flatness finesse, $\mathscr{F}_{flat}$, of the filter mirrors, which for curvature nonflatness[5] is given by

$$\mathscr{F}_{flat} = \frac{M_1}{2} , \tag{30}$$

where the curvature error is λ/M_1. For $\lambda/200$ plates, this sets a limiting finesse of 100 for any FP. The second is the reflectivity finesse, $\mathscr{F}_{fr}$, given by Eq. (8):

$$\mathscr{F}_{fr} = \frac{\pi\sqrt{R_f}}{1 - R_f} , \tag{31}$$

where R_f is the common reflectivity for both mirrors. The net finesse of the filter, $\mathscr{F}_{filt}$, is given by

$$\mathscr{F}_{filt}^2 = \mathscr{F}_{flat}^2 + \mathscr{F}_{fr}^2 . \tag{32}$$

The finesse of the filter broadens the analyzer FP pattern. If the oscillator emitted a continuum of frequencies, rather than the distinct modes shown in Fig. 6, then light of frequencies v_{10} and v_{20} would be available and would produce fringe patterns after the analyzer FP that overlap almost perfectly.

Now consider the distinct oscillator modes of Fig. 6. Since v_{10} and v_{20} are almost exactly equivalent in the final fringe pattern, it is seen that the position of the v_m light depends mostly upon the difference $v_{10} - v_m$ and not upon v_m itself. Here v_{10} is the peak frequency of the 0-deg transmission pattern that is nearest to the frequency v_m. Since the oscillator modes completely sample an entire FSR of the filter's 0-deg transmission curve, the analyzer fringe pattern is broadened by the filter. This broadening, which is for the 0-deg oscillator light only, makes the limiting finesse of the final fringe pattern equal to that of the filter.

Thus we see that the broadening of the fringe pattern due to the 0-deg light is just the same as if the oscillator emitted a continuum of frequencies covering just one FSR of the filter.

B. Angular Divergence of the Light

The angular divergence of light exiting the telescope also broadens the fringe pattern. We give two approaches to evaluating this effect. Figure 6 shows that for finite angles, higher frequencies can be transmitted. For our applications, the largest angle θ_0/M entering the filter will be so small that, even

11

though the difference $v_1(\theta_0/M) - v_{10}$ is significant compared to 75 MHz, the fractional change in the FSR due to the cos (θ) term is negligible compared to the finesse of the filter.

The oscillator will completely populate the entire T(θ) curve of Fig. 6 as well, further broadening the final fringe pattern. Even though the actual oscillator frequencies that fall near transmission peaks may be widely separated, the effect on the analyzer fringe pattern is the same as if there were a continuum of source frequencies spanning one FSR of the filter. Thus one can think of the various transmitted frequencies as producing an effective bandwidth, EBW, that is somewhat broader than that due to the filter finesse. We deduce the combined broadening due to light of all angles by convolving the 0-deg transmission curve, expressed as a function of phase, or v cos (θ) with the assumed angular distribution of light incident upon the filter.

We assume the incident light per unit solid angle is constant between 0 deg and the maximum angle $\theta_m = \theta_0/M$. The incident light is then given by

$$\frac{dI}{dv d\theta} = \frac{\sin\theta}{\Delta v\left(1 - \cos\theta_m\right)} \tag{33}$$

and has unit total intensity, since

$$\int\int \frac{dI}{dv d\theta} d\,v\,d\,\Omega = 1 \quad . \tag{34}$$

These results correspond to the distributions shown in Fig. 7. This distribution is then convolved with the transmission curve, Eq. (10), to give the distribution of effective frequencies at the output of the filter

$$\frac{d\,I}{d\,v}\Big|_{out} = \frac{\left(1 - \dfrac{A}{1 - R}\right)^2}{\Delta v\left(1 - \cos\theta_m\right)} \int_0^{\theta_m} \frac{\sin\theta\,d\theta}{1 + \dfrac{4R\sin^2\delta/2}{(1 - R)^2}} \quad . \tag{35}$$

Here we are adding the effects of different angles incoherently, since we want Eq. (35) to represent the angle-integrated frequency spectrum.

The result of the integration is that

$$\frac{d\,I}{d\,v}\Big|_{out} = \frac{s}{v}\left\{\tan^{-1}\left[\mu\tan\left(L\,v\right)\right] - \tan^{-1}\left[\mu\tan\left(L\,v\cos\theta_m\right)\right]\right\} \quad , \tag{36}$$

where

$$s = \frac{\left(1 - \dfrac{A}{1 - R}\right)^2}{\mu\,L\,\Delta\,v\left(1 - \cos\theta_m\right)} \quad , \tag{37}$$

$$L = \frac{2\pi h_f}{c} \quad , \tag{38}$$

and

$$\mu = \frac{1 + R}{1 - R} \quad . \tag{39}$$

Equation (36) is best used by rewriting it in another form. Since the frequency v_{10} of Fig. 6 is resonant at 0 deg, it obeys the relation

$$L v_{10} = n\pi \quad , \tag{40}$$

12

where n is an integer. Then Eq. (36) can be written

$$\frac{d\,I}{d\,\nu}\Big|_{out} = \frac{s}{\nu}\left(\tan^{-1}\left\{\mu\tan\left[L\left(\nu - \nu_{10}\right)\right]\right\} - \tan^{-1}\left\{\mu\tan\left[L\left(\nu\cos\theta_m - \nu_{10}\right)\right]\right\}\right) \quad . \tag{41}$$

To properly use Eq. (41), both arguments of the tangents must have an absolute value less than $\pi/2$, which means that the frequencies considered must be within 0.5 FSR of ν_{10} and that

$$\theta_m^2 < \frac{\lambda}{2\,h_f} \quad . \tag{42}$$

Both conditions are easily met for our application, since neither the frequencies considered nor the angular divergence will necessitate evaluating the distribution at frequencies farther than 0.5 FSR away from ν_{10}.

Equation (41) is a rigorous result in the continuum model but is not illuminating physically. We now give a simpler method of deriving the broadening due to both the finesse and the angular divergence. The effective bandwidth for transmitted 0-deg light is simply

$$E\,B\,W = \frac{c}{2\,h_f\,\mathscr{F}_{filt}} \quad . \tag{43}$$

This is 75 MHz for the example in Fig. 6. Since ν_{10} is resonant at 0 deg, the peaks of the transmission curves for $\theta \neq 0$ will obey

$$\nu_{10} = \nu\cos\theta = \nu_{max}\cos\theta_m \quad . \tag{44}$$

Let the maximum angle θ_m correspond to the highest peak transmission frequency ν_{max}. Then the difference in peak transmission frequencies is just

$$\nu_{max} - \nu_{10} = \nu_{max}\left(1 - \cos\theta_m\right) \doteq \frac{\nu_{max}\,\theta_m^2}{2} \doteq \frac{\nu_{10}\,\theta_m^2}{2} \doteq \frac{c\,\theta_m^2}{2\,\lambda_0} \quad . \tag{45}$$

A rough estimate for the total effective bandwidth due to both the finesse and angular divergence can be made by adding in quadrature the contributions of Eqs. (43) and (45). This gives, after some rearrangement, the simple result for its full width at half-maximum:

$$FWHM\left(\frac{dI}{d\nu}\Big|_{out}\right) \doteq \frac{c}{2\,h_f\,\mathscr{F}_{filt}}\sqrt{1 + \left(\frac{\mathscr{F}_{filt}\,h_f\,\theta_m^2}{\lambda_0}\right)^2} \equiv \frac{c}{2\,h_f\,\mathscr{F}_{filt}}\sqrt{1 + \left(\frac{\mathscr{F}_{filt}}{\mathscr{F}_\theta}\right)^2} \quad . \tag{46}$$

The derivation of Eqs. (46) and (41) assumed that the beam centroid angle was at 0 deg. If not, then the same angular divergence makes more broadening than these results indicate.

C. Comparison of the Two Results

One evaluates Eq. (41) over a range of frequencies to determine a rigorous value for the FWHM of the output frequency distribution, and thus a net finesse including divergence can be calculated. This has been done numerically, and it is found that Eq. (46) is a very excellent approximation to the correct FWHM. For example, for $\mathscr{F}_{filt} = 33$ and an angular divergence that drops the net finesse down to 18.22, the simple estimate Eq. (46) gives 18.24. In fact, for net finesses ranging from 33 for no divergence to 2.7 for very large divergence, the two methods always agree to within 1%. We do not understand why this should be the case. Equation (41) included the assumed angular distribution of light from Eq. (43), but Eq. (46) does not even specify the particular angular distribution.

The close agreement of Eq. (46) with the correct result is fortunate, since it is more easily included in simple calculations. We may simply consider the angular divergence as another source of finesse given by

$$\mathscr{F}_\theta = \frac{\lambda}{h_f \, \theta_m^2} \quad . \tag{47}$$

Then the reciprocals of the flatness, reflectivity, and angular divergence finesses can be added in quadrature. We desire to make θ_m small enough so that the angular divergence doesn't significantly broaden the fringes. This will occur if

$$\mathscr{F}_\theta > 2 \, \mathscr{F}_{filt} \, , \quad \text{or} \quad \theta_m^2 < \frac{\lambda}{2 \, h_f \, \mathscr{F}_{filt}} \quad . \tag{48}$$

D. Walkoff in the Filter

In some instances, additional broadening may occur in the filter if its diameter is too small. As shown by Roychoudhuri[8] and in Ref. 1, the intensity of the light at a resonant angle increases with time as the number of multiply reflected beamlets N increases. The intensity increases as

$$I = (1 - R^N)^2 \quad , \tag{49}$$

where R is the reflectivity. For R exceeding 0.9 the intensity reaches 90% and 99.7% of its final value after about $\mathscr{F}_{filt}$ and $2\mathscr{F}_{filt}$ beamlets have formed, respectively. Thus the transverse walk for the largest angle in the beam is

$$\text{Walk} = 2 \, h_f \, \theta_m \cdot 2 \, \mathscr{F}_{filt} \quad . \tag{50}$$

If the edge of the incident beam is closer to the edge of the mirrors than this, some additional broadening will occur. However, usually the maximum angle will obey Eq. (48), so that the walk would be less than

$$\sqrt{8 \, \lambda \, h_f \, \mathscr{F}_{filt}} \quad . \tag{51}$$

This is usually quite small. For example for $h_f = 6.5$ cm, $R_f = 0.91$, and perfectly flat mirrors, the walk is less than 0.3 cm for green light. Thus walkoff in the filter is not usually a problem.

E. Walkoff in the Analyzer

Walkoff in the analyzer is more important than in the filter. This is because the stripe in the center of the analyzer mirror reduces the transverse walk that the edge of the beam can undergo before reaching the edge of the mirror. Also the reflectivity of the analyzer may be larger than that of the filter.

Equation (20) of Ref. 1 gives the intensity pattern as a function of time, angle, and reflectivity for a lossless, normal, unstriped FP. A similar expression, but including absorption, is found in Eqs. (5.3.25) and (5.3.26) of Ref. 5. A discussion of walkoff for unstriped FPs is given by Van der Sluis and McNally.[9] From these results it is very straightforward to generalize our Eq. (21) for incoherent illumination of a striped FP to include the effects of walkoff and absorption. The result, for $R_1 = 1$, is

$$I = T_2 \left[1 - q + q \left(\frac{1 - R^N}{1 - R} \right)^2 \frac{1 + \dfrac{4 \, R^N \sin^2 N \, \delta/2}{(1 - R^N)^2}}{1 + \dfrac{4 \, R \sin^2 \delta/2}{(1 - R)^2}} \right] \, , \tag{52}$$

14

where T_2 is defined by Eq. (5) and N is the number of beamlets exiting the second mirror. For a striped circular mirror of radius R_{fp}, an illumination filling the entire length and width of the stripe has an effective distance = 0.78 R_{fp} transverse to the edge of the mirror. Thus the number of beamlets, N, is approximately

$$N \doteq INT\left(\frac{0.78\, R_{fp}}{2\, h_a\, \theta}\right) \quad . \tag{53}$$

We have evaluated the FWHM of the expression given by Eq. (52) for a wide range of parameters to determine the combined finesse due to both walkoff and reflectivity. We have found a simple analytical formula that is a good approximation to that FWHM for a striped set of 2.5-cm-radius mirrors. For $R_a < 0.97$, $h_a < 15$ cm, and for the first three fringes formed, the FWHM of Eq. (52), denoted $\mathscr{F}_{arw}$, is within 3% of the simple estimate

$$\mathscr{F}_{arw} \doteq \mathscr{F}_{ar}\frac{\left(1 - R_a^{0.8N}\right)^2}{1 - R_a^{2N}} \tag{54}$$

for the combined finesse including walkoff and reflectivity. Here $\mathscr{F}_{ar}$ is the analyzer finesse due to reflectivity only, given by Eq. (8). In addition to $\mathscr{F}_{arw}$, the total finesse of the analyzer includes a flatness term similar to Eq. (30). The effect of walkoff increases as R approaches unity and h_a increases. For example, for $R_{fp} = 2.5$ cm, R = 0.97, and $\lambda = 5145$ Å, the reflectivity finesse is 101.5 and the combined effects of reflectivity and walkoff are shown for $h_a = 6.5$ and 15 cm in Table I.

The method used to find Eq. (54) was first to assume that the total energy exiting a striped FP of finite size with $R_1 = 1$ was a constant k times the peak intensity times the FWHM. The expression for the energy in the remaining beamlets that walk off the mirrors was assumed to use the same constant k. The sum of these two energies was then set equal to the energy exiting the FP if the mirrors had been very large, still using the same constant k. This procedure would give the correct FWHM of Eq. (52) provided the shape of all the transmission patterns were similar. They are not, and the poor quality of the model derived by the above technique reflected that. However, if the number multiplying N in the numerator of Eq. (54) is changed from unity to 0.8 as shown, the model becomes very good!

F. The Overlap Finesse

If the frequencies transmitted by the filter were very narrow due to very high filter flatness and reflectivity finesse and very low angular divergence, the nonperfect overlap of the fringes at the analyzer causes what is called, in Ref. 2, the overlap finesse. Detailed formulas for the overlap finesse and fringe angles for the clusters of fringes formed are given by Goosman,[6] and some of those results are repeated here.

Define the average, minimum, and maximum mode numbers m by

$$m_{av} = \frac{2\, h_f}{\lambda_{av}} \;,\; m_{min} = \frac{2\, h_f}{\lambda_{max}} \;,\; m_{max} = \frac{2\, h_f}{\lambda_{min}} \quad . \tag{55}$$

As detailed in Ref. 6, complete groups of $m_{max} - m_{min}$ fringes clustered close together are assigned cluster numbers J. The innermost complete cluster has J = 1, the next has J = 2, etc. Depending upon the values of the quantities

$$\delta_1 = \frac{h_a - h_f}{h_f} \tag{56}$$

and x_1, defined by

$$x_1 = \delta_1 + \frac{2V}{c} \quad , \tag{57}$$

15

there may be an incomplete group of fringes, near 0 deg, that is not assigned a cluster number.

To determine the overlap finesse we define, as in Ref. 6, the quantity

$$J_0 = 1 + INT\left(x_1 \, m_{min}\right) \qquad \text{for } x_1 \geq 0 \tag{58}$$

and

$$J_0 = - INT\left| x_1 \, m_{max}\right| \qquad \text{for } x_1 < 0 \quad . \tag{59}$$

The results of Ref. 6 allow us to express the angles for the centroids of the clusters as

$$\theta\left(J, m_{av}\right) \doteq \sqrt{\frac{\lambda_{av}\left(J + \epsilon_1\right)}{h_f}} \quad , \tag{60}$$

where ϵ_1 is

$$\epsilon_1 = x_1 \, m_{av} - J_0 \quad . \tag{61}$$

Equation (60), for multifrequency operation, is similar to but not the same as Eqs. (6) and (7) for single-frequency operation. The difference results from the fact that, due to an incomplete cluster near 0 deg, the centroid angle of the first complete cluster may correspond to the second ring for the centroid frequency. Therefore the $J = 1$ cluster may have $J + \epsilon_1$ exceeding unity, but for most values of x_1 the quantity $1 + \epsilon_1$ will be between 0 and unity. Therefore we may relate the j of Eqs. (6) and (7) to the cluster number J here by

$$J + \epsilon_1 = j = k - 1 + \epsilon \quad . \tag{62}$$

As shown in Ref. 6, if $x_1 \geq 0$, J_0 is the unbroadened cluster number. Note that the unbroadened cluster number, if it exists, depends upon the reflector velocity V. If x_1 is negative, there is no unbroadened cluster, but the above definition of J_0 is useful since we can write the overlap finesse as

$$\mathscr{F}_{OL} = \frac{\lambda_{av}}{\lambda_{max} - \lambda_{min}} \frac{1}{\left| J - J_0 \right|} \quad , \tag{63}$$

regardless of the sign of x_1. For example, with $\lambda_{ave}/(\lambda_{max} - \lambda_{min}) = 250$, the overlap finesse is greater than 50 for clusters J that are less than 5 away from the unbroadened cluster.

G. Diffraction Broadening?

The finite size of the beam at the spherical lens might be considered to impose a diffraction limit on the waist size of the light at the stripe. The size of the illumination at the spherical lens in the x direction (see Fig. 1) is approximately the transverse walk per beamlet multiplied by the number of beamlets

$$D_{i\ell\ell} \doteq 2 \, h_a \, \theta_j \, \mathscr{F}_{arw} \quad , \tag{64}$$

where the FP finesse, $\mathscr{F}_{arw}$, represents, for flat mirrors, the number of beamlets required to produce a nearly complete interference pattern.

Far-field diffraction from a rectangular opening of size D implies an angular spread half-width about the centroid angle θ_j of

$$\Delta\,\theta_j \doteq \frac{\lambda}{2\,D_{i\ell\ell}} \quad , \tag{65}$$

16

where we have neglected the complication of speckle.

Thus we might consider constructing a diffraction-limited finesse defined as

$$\mathscr{F}_D = \frac{\theta_{j+1}^2 - \theta_j^2}{(\theta_j + \Delta\theta_j)^2 - (\theta_j - \Delta\theta_j)^2} \doteq \frac{\lambda}{4\,h_a\,\theta_j\,\Delta\theta_j} = \mathscr{F}_{arw} \quad . \tag{66}$$

It can be seen that the diffraction-limited finesse is approximately equal to the FP finesse! This diffraction-limited finesse should be ignored, however, since the derivation of the FP finesse implicitly takes into account diffraction, and we would otherwise be double counting. As proof of this, we noted in Section II.C that a detailed treatment using Gaussian beamlets rather than rays produces the normal finesse expected from the ray treatment.

Note that the size of the illumination at the spherical lens, as given by Eq. (64), is automatically made large enough to satisfy the usual diffraction-limited, focussed spot size.

H. Slit Finesse

The final two broadening sources, the curvature of the streaking camera slit and the spatial resolution of the streaking camera, are converted to equivalent finesses. From Eq. (66) we see that if $\Delta\theta_{j,HWHM}$ is the HWHM of the angular spread of fringe j due to some source of broadening, the finesse associated with that source is

$$\mathscr{F}(j) = \frac{\lambda}{4\,h\,\theta_j\,(\Delta\theta_{j,HWHM})} \quad . \tag{67}$$

The half-width of the streaking-camera slit in the x direction, denoted by R_x, usually determines the focal length, FL, of the spherical lens, since we usually desire to have about four fringe pairs fill the slit. We define an integer p_{slit} by the relation

$$R_x = FL\sqrt{\frac{\lambda\,p_{slit}}{h_a}} \quad . \tag{68}$$

p_{slit} will usually be about four but may differ somewhat due to the unavailability of certain focal lengths. The FWHM of fringe j at the slit, denoted by w(j), then equals FL times twice the half-angular width $\Delta\theta_{j,HWHM}$. Using Eq. (6) we then can write the finesse of the jth fringe as

$$\mathscr{F}(j) = \frac{R_x}{2\,w(j)\,\sqrt{j}\,p_{slit}} \quad . \tag{69}$$

For a streaking camera slit of half-width R_x and half-height R_y it is easy to show that the full extent of the fringe width due to the curvature of the circular fringes and the finite size of R_y is approximately[10,1]

$$w(j) \doteq \frac{R_y^2}{2\,x_j} \quad . \tag{70}$$

The above results then mean that the slit finesse, $\mathscr{F}_{slit}$, is

$$\mathscr{F}_{slit} = \frac{R_x^2}{R_y^2\,p_{slit}} \quad , \tag{71}$$

which is independent of fringe number j, as noted in Ref. 10.

17

I. Streaking-Camera Spatial Resolution

The streaking-camera magnification from slit to phosphor is denoted as *magcam*, and the spatial resolution of the camera at the phosphor is called *dxcam*. Then, using Eq. (69), we see that the camera finesse is

$$\mathscr{F}_{cam} = \frac{R_x \cdot magcam}{4\sqrt{j}\ dxcam} \quad . \tag{72}$$

J. Total Finesse and Velocity Resolution

We approximate the total finesse of the entire system by quadrature addition of the individual finesses. A more exact treatment would do the convolutions correctly. Thus the total finesse of fringe j is

$$\mathscr{F}_{tot} = \left(\mathscr{F}_{filt}^{-2} + \mathscr{F}_{\theta}^{-2} + \mathscr{F}_{OL}^{-2} + \mathscr{F}_{arw}^{-2} + \mathscr{F}_{flat}^{-2} + \mathscr{F}_{slit}^{-2} + \mathscr{F}_{cam}^{-2}\right)^{-0.5} \quad , \tag{73}$$

where the contributions come from Eqs. (32), (47), (63), (54), (30), (71), and (72), respectively.

Reference 1 and others show that the velocity, V_{fsr}, corresponding to one FSR range is

$$V_{fsr} = \frac{c\,\lambda}{4\,h_a} \quad . \tag{74}$$

A simple estimate of the velocity resolution, ignoring intensity considerations, is to treat the HWHM of the fringe as the limiting accuracy. This means that the minimum resolvable velocity, V_{min}, is

$$V_{min} \doteq HWHM = \frac{V_{fsr}}{2\,\mathscr{F}_{tot}} \quad . \tag{75}$$

This result assumes that sufficient light is available at the streaking camera. Otherwise limited photocathode statistics further broaden the fringes.

V. Time Resolution

We consider four contributions to the time resolution of the system. The streaking camera has a limiting time resolution, *dtcam*, caused partly by photoelectron transit-time spreading. It is independent of the streaking speed and of the spatial resolution of the camera measured at the phosphor, denoted by *sscam* and *dxcam*, respectively. The time resolution caused by spatial resolution is

$$TR_{space} = \frac{dxcam}{sscam} \quad . \tag{76}$$

The time resolution due to the finite size of the slit is the time it takes the image of the slit on the phosphor to move by its own full width, or

$$TR_{slit} = \frac{2\,R_y\,magcam}{sscam} \quad . \tag{77}$$

The last contribution is the fill time of the FP mirrors. For mirrors of infinitely large diameter this topic is treated by several authors.[1,5,8] We derive an expression here that includes the effect of walkoff for finite-sized mirrors. The second term in Eq. (52) represents intensity vs angle as a function of the number of

beamlets N, as expressed by Eq. (53). Because of its dependence on the angle, N is a function of fringe number j. Each beamlet represents a time increment of

$$t_0 = \frac{2\,h_a \cos\theta}{c} \quad .$$

(78)

Since the sine terms of Eq. (52) vanish at resonant angles, we can easily find the time required for the intensity to reach a fraction g of the intensity that a finite number of beams N_j would eventually make. This is done by setting

$$\left(1 - R^{T_j}\right)^2 = g\left(1 - R^N\right)^2 \quad ,$$

(79)

where the quantity T_1 is defined in terms of the fill-time τ by

$$T_1 = \text{INT}\left(\frac{\tau}{t_0}\right) \quad .$$

(80)

Equations (79) and (80) are solved for the fill-time, including the effects of finite mirror size, yielding

$$\tau_j = \frac{2\,h_a \cos\theta_j}{c}\;\frac{1\,n\left[1 - \sqrt{g}\left(1 - R^{N_j}\right)\right]}{1\,n\,R} \quad .$$

(81)

The fill-time depends on fringe number j. If N_j is set to infinity, representing large mirrors, Eq. (81) reduces to the result of Burgess,[11] as reproduced in Ref. 1.

Thus the total time resolution of the entire system is approximately

$$TR = \sqrt{d\,t\,cam^2 + TR_{slit}^2 + TR_{space}^2 + \tau_j^2} \quad .$$

(82)

VI. Relative Photographic Writing Speed of Each Fringe

The above formulas allow estimation of both the velocity and time resolution for each fringe for a given configuration, ignoring any light-intensity effects. Since experiments are often light-limited, one also needs an estimate of the relative light intensity of each fringe. In this section we estimate the relative photographic writing speed of each fringe so that users may easily estimate the penalty in intensity associated with improving either the time or velocity resolution. A complete treatment of this problem is complex, due to the finite size of illumination on the reflector and the latter's travel distance. However, several useful conclusions can be drawn simply on the basis of emittance or brightness arguments. The rough approximations outlined below leave much room for further refinement.

We estimate first the energy content of each fringe used by the entire optical system for unit energy emitted by the oscillator. We will express the result as the product of four fractions FR_1 through FR_4. We then will estimate the relative peak intensities by dividing the fringe energy content by the total width of the fringe.

The power fraction FR_1 passed by the filter, from Eq. (12), is

$$FR_1 = \left(1 - \frac{A}{1 - R_f}\right)^2 \frac{1 - R_f}{1 + R_f} \quad ,$$

(83)

where R_f is the reflectivity of the filter mirrors. However, only a portion of this power is usable, since the power between resonances does not contribute to the intensity of peaks in the analyzer pattern. We take the useful power as that fraction of the frequency spectrum emitted by the filter that lies within the range

19

$$v_{peak} - \frac{c}{2\,h_f\,\mathscr{F}_{tot}} \leq v \leq v_{peak} + \frac{c}{2\,h_f\,\mathscr{F}_{tot}} \quad . \tag{84}$$

Since we expand the beam at the filter, walkoff is negligible. However, we still include the flatness contribution to its finesse by using a transmission determined by Eq. (9), where for R we substitute an effective reflectivity R_{eff}, defined by

$$R_{eff} = 1 + \frac{\pi^2}{2\,\mathscr{F}_{filt}^2} - \frac{\pi}{\mathscr{F}_{filt}} \sqrt{1 + \frac{\pi^2}{4\,\mathscr{F}_{filt}^2}} \quad . \tag{85}$$

This makes the filter finesse, including flatness, obey the relation

$$\mathscr{F}_{filt} = \frac{\pi\sqrt{R_{eff}}}{1 - R_{eff}} \tag{86}$$

as in Eq. (8). Then the fraction FR_2 of the filtered power that is useful and obeys Eq. (84), obtained by integration, is

$$FR_2 = \frac{2}{\pi} \tan^{-1}\left[\frac{1 + R_{eff}}{1 - R_{eff}} \tan\left(\frac{\pi}{\mathscr{F}_{tot}}\right)\right] \doteq \frac{2}{\pi} \tan^{-1}\left(\frac{2\,\mathscr{F}_{filt}}{\mathscr{F}_{tot}}\right) \quad , \tag{87}$$

the latter form being approximate for large finesses.

We assume that the reflector is located at the illumination waist of radius R_{tgt}. This will not be exactly true if the target moves significantly compared to the depth of field of the illumination optics. Thus we redefine R_{tgt} to be the square root of the distance-averaged square of the spot size on the reflector. We further assume that the reflected light is uniformly intense in position out to radius R_{tgt}, with an angular distribution uniform in solid angle out to an angle θ_{tgt}, and that the angular distribution is the same for all illuminated points of the reflector.

We simplify the problem by assuming that the illumination made by the cylinder lens comes to a waist at the stripe and is larger than it. We also assume, as above, that the light is spatially incoherent and the angular distribution of light at the stripe is independent of radius and symmetric in the x coordinate (Fig. 2). The light intensity is uniform in angle from the axis out to the angle given by Eq. (23), which defines the quantity p_{cyl}. We further assume that the illumination is at a waist at the slit of the streaking camera, as well as at the reflector and at the stripe.

Regardless of how the light from the reflector is transported to the stripe, if the above assumptions hold then we can give an upper limit to the fraction of light illuminating the target that can pass through the stripe and the slit of the streaking camera. We use simple emittance or brightness arguments, since the light energy per unit area per unit solid angle cannot be increased by the optical transport system between reflector and stripe.

At the reflector, the emittance of the reflected light is simply the square of the product of its radius and half-angle. The emittance acceptance of the stripe and the slit is factorable into parts. The first is the product of R_{st}, and the maximum angle of illumation at the stripe given by Eq. (23). The second is the product of the half-height of the slit, R_y, and the maximum vertical angle of illumination at the slit. The latter is about 0.8 times the FP mirror radius, R_{fp}, divided by the focal length, F_L, of the spherical lens. Thus the largest fraction of the reflected light that can pass through the stripe and the slit (neglecting the analyzer FP for the moment) is simply

$$FR_3 = \frac{R_{st}\,\theta_{cyl}\,R_y\,0.8\,R_{fp}}{R_{tgt}^2\,\theta_{tgt}^2\,FL} \quad . \tag{88}$$

The actual dynamic shocked reflectivity of the target is not included, since it is assumed to not be in the control of the experimenter. Equation (88) is an upper limit. By writing a separate optical transport code for a

field lens plus fiber-optic coupling between reflector and the stripe, we have been able to achieve fractions between 25% and 70% of this limit for targets moving about 10% of the distance to the first field lens.

Equation (88) can be rewritten in a simpler form by substituting Eq. (68) for the focal length F_L, by setting $p_{str} = p_{cyl} = p_{slit} = 4$, and by using Eq. (74). The result is

$$FR_3 = \frac{12.8 \sqrt{\frac{V_{fsr}}{c}} R_{fp} R_y \lambda}{R_{tgt}^2 \theta_{tgt}^2 R_x} \quad . \tag{89}$$

Thus the FP is more efficient in light collection for large slit heights, short slits, large mirror radii, and large velocities per fringe. Short slits allow short-focal-length spherical lenses, for a fixed number of fringes, which in turn increase the amount of acceptable vertical angular divergence. Small spot sizes on the reflector and small reflected angular divergences are easier to collect. Equation (89) is just the ratio of emittance acceptance to reflected target emittance.

The counter-effect of most of the intensity-enhancing parameters shown in Eq. (89) is clear. Because of the limited resolution of the streaking camera, short slits reduce velocity resolution. Large slit heights compromise time resolution, and large V_{fsr} values compromise velocity resolution. However, large-radii mirrors are beneficial.

We now ask how much of this light that is accepted by both the stripe and the slit is lost in the striped FP and how much is portioned among the various fringes. The fringes and the quantities denoting them are illustrated in Fig. 3. The descriptors j, k, and ϵ are defined by Eqs. (6) and (7). The maximum number of fringe pairs, k_{max}, is difficult to determine in the completely general situation. If the stripe width is as recommended, with $p_{str} = 4 = p_{cyl}$, then k_{max} is roughly one more than the integer value of p_{cyl}, due to diffraction as discussed in Section II.C. If p_{str} is much less than p_{cyl}, then k_{max} will exceed $p_{cyl} + 1$.

We now determine FR_4, the ratio of energy content of a single fringe dot to the total energy capable of entering the stripe and slit. An approximate method is to take the product of the peak intensity of the resonant part of Eq. (52) times the FWHM of that peak as being proportional to the energy content of that dot. The FWHM of the peak in angle space is given by

$$\Delta \theta_j = \frac{1}{2 \mathscr{F}_{arw}} \sqrt{\frac{\lambda}{j \, h_a}} \quad , \tag{90}$$

and the energy content of the dot is proportional to

$$E_j = T_2 \, q \left(\frac{1 - R^{N_j}}{1 - R}\right)^2 \Delta \theta_j \quad . \tag{91}$$

Using the same proportionality, we obtain the energy capable of entering the stripe and the slit by summing, over all the fringe dots, the product of peak intensity times FWHM. However, we now set A = 0, q = 1, $N_j = \infty$, and use $\mathscr{F}_{ar}$ in Eq. (90) to determine the dot width. Thus this quantity, denoted E_{den}, is approximately

$$E_{den} = 2 \sum_{k=1}^{k_{max}} \frac{1 - R_2}{(1 - R)^2} \sqrt{\frac{\lambda}{h_a \, j(k)}} \frac{1}{2 \mathscr{F}_{ar}} \quad . \tag{92}$$

The initial factor of two in Eq. (92) is due to there being two dots for a given j for a symmetric pattern. The desired ratio is then

$$FR_4 = \frac{E_j}{E_{den}} \quad . \tag{93}$$

Note that the effect of nonflat mirrors has been ignored in Eqs. (90) and (91). The finese is lowered, as mentioned just below Eq. (54), and the peak height is reduced. Neither effect is included in Eq. (91), since

21

$\mathscr{F}_{arw}$ does not include flatness. One might further refine Eq. (91) by substituting the total analyzer finesse for $\mathscr{F}_{arw}$ in Eq. (90) and including a term in Eq. (91) to express the reduction of peak height. The latter is a complex topic, and is discussed in Sec. 2.3 of Ref. 5. However, neglecting flatness effects on both the height and the width is better than neglecting only the effect on the height, since some compensation occurs.

Thus the energy in a dot divided by the oscillator output energy is proportional to

$$FR = FR_1 \, FR_2 \, FR_3 \, FR_4 \quad . \tag{94}$$

The photographic writing speed on the streaking camera for a dot is the energy per unit area emitted by the phosphor of the streaking camera. This is the product of FR times the energy gain of the camera from slit to phosphor, denoted E_{gain}, times the energy per unit area per unit time at the slit multiplied by the time for the image of the slit to sweep past itself on the phosphor. The FWHM of the fringe at the slit is

$$FWHM = FL \sqrt{\frac{\lambda}{j \, h_a}} \, \frac{1}{2 \, \mathscr{F}_{tot}} \quad , \tag{95}$$

in analogy with Eq. (90). Using Eq. (68) for the focal length of the spherical lens, FL, we deduce the limiting photographic writing speed as

$$PWS_j = \frac{4 \, FR \cdot E_{gain} \cdot \sqrt{j \, P_{slit}} \, \mathscr{F}_{tot}(j)}{R_x \cdot magcam \cdot sscam} \quad . \tag{96}$$

Equation (96) represents the upper limit to the photographic writing speed for each dot j, under the assumptions listed above, for a reflector with unit reflectivity integrated over angle. It is most useful for situations where the optics illuminating the reflector and the optics transporting reflected light to the stripe are held constant, and only the sizes of the stripe and slit, the reflectivities, the oscillator angular divergence, and the flatness, diameters, and spacings of the FP mirrors are varied.

VII.   Nonstriped FP and Single-Frequency Operation

If nonstriped mirrors are used, then the above results may still be used, provided the following modifications are made. All intensities are multiplied by the ratio of Eq. (10) to Eq. (3). The reflecting fraction of Eq. (20) is set equal to unity. Finally, the 0.78 factor in Eq. (53) should be increased to about 1.5, depending upon the illumination condition, to account for less walkoff in the analyzer FP.

If single-frequency laser illumination is used, then the overlap, filter, and angular-divergence finesse terms in Eq. (73) should be dropped and replaced by a term representing the bandwidth of the laser, and one should set $FR_1 = FR_2 = 1$.

VIII.   Conclusions

We have presented simple analytical approximations for the velocity and time resolution of each fringe. The basic assumptions in deriving these results were that the illumination is sufficient to make photocathode statistics ignorable and that the illumination at the stripe is spatially incoherent and larger than the stripe, with no correlation between position and angle. Many of the results assumed that $R_1 = 1$. We convolved all the contributions in quadrature, but the results for the individual contributions to velocity and time resolution could be, in a more refined treatment, convolved properly.

We have derived an expression showing how the upper limit on the photographic writing speed of each fringe depends on most of the variables in the optical configuration.

We have given a recipe for using these results for unstriped FPs, along with an explanation of the role of diffraction in energy conservation.

Acknowledgments

References

1. C. F. McMillan, D. R. Goosman, N. L. Parker, L. L. Steinmetz, H. H. Chau, T. Huen, R. K. Whipkey, and S. J. Perry, *Rev. Sci. Instrum.* **59**, 1 (1988).
2. S. Gidon and G. Behar, *Appl. Opt.* **27**, 2315 (1988).
3. C. F. McMillan, N. L. Parker, and D. R. Goosman, *Appl. Opt.* **28**, 826 (1989).
4. M. Born and E. Wolf, *Principles of Optics* (Pergamon, New York, 1983), Chap. 7.
5. G. Hernandez, *Fabry-Perot Interferometers* (Cambridge University Press, Cambridge, 1986), p. 150.
6. D. R. Goosman, *Dynamic Fringe Broadening in Multi-Line Laser Doppler Velocimetry*, Lawrence Livermore National Laboratory, Livermore, CA, UCRL-99478 (1988).
7. C. F. McMillan, Lawrence Livermore National Laboratory, Livermore, CA, private communication, 1988.
8. C. Roychoudhuri, *J. Opt. Soc. Am.* **65**, 1418 (1975).
9. K. L. Van der Sluis and J. R. McNally, *J. Opt. Soc. Am.* **46**, 39 (1956).
10. D. J. Bradley, B. Bates, C. O. L. Juulman, and S. Majumdar, *Appl. Opt.* **3**, 1461 (1964).
11. T. J. Burgess, *Photon Fill-Time of a Fabry-Perot Spectrometer*, Lawrence Livermore National Laboratory, Livermore, CA, UCID-15224 (1967).

FIGURE CAPTIONS

Figure 1. The optical configuration considered consists of an oscillator, telescope, filter FP interferometer, reflecting target, optical transport system, cylinder lens, striped analyzer FP of nearly the same spacing as the filter, spherical lens, and electronic streaking camera. The oscillator emits a beam whose FWHM is $d\lambda$, centered about wavelength λ_0 with a radius R_0 and beam divergence half-angle of θ_0. This divergence is reduced by the telescope magnification M to reduce the bandwidth emitted by the filter FP. The filtered light is transported onto the surface of a moving reflector with an illumination spot radius R_{tgt} that reflects light with an angular-divergence half-angle of θ_{tgt}. An unspecified optical transport system carries some of the light to a cylinder lens, which produces a waist of radius R_{ill} at the striped entry mirror of the analyzer FP of reflectivities R_1 and R_2. The analysed beam is focused by the spherical lens of focal length FL onto the slit of the electronic camera, whose openings in the x and y directions are $2R_x$ and $2R_y$, respectively. The electronic camera magnifies the image at the slit by a factor *magcam* at the phosphor and sweeps the slit image with a speed *sscam* across the phosphor.

Figure 2. A single ray of light enters a lossless, flat, very-large-diameter set of FP mirrors of reflectivities R_1 and R_2, respectively. The ray enters with angle θ and crosses the plane of the first mirror a distance x from the center of the stripe of half-width R_{st}, where the mirror coating has been removed. The amplitudes of the first three beamlets formed are shown in terms of the amplitude transmittances and reflectivities t_1, t_2, r_1, and r_2.

Figure 3. Labeling of the fringes, which are shown as a function of angle. (a) Zero deg is not resonant. (b) Zero deg is resonant.

Figure 4. A Gaussian beam with centroid angle θ_j and waist radius R_0 enters the stripe of half-width somewhat larger than R_0. The beam divergence half-angle is θ_b. The mirror separation is h.

Figure 5. A finite-sized beam entering a normal FP, producing exiting beamlets that do not necessarily overlap well spatially. As shown in the text, if the incident beam is large enough to cause the beamlets to overlap well, then the angular spread of the beam is small compared with an FSR, and good energy transmission can occur.

Figure 6. (a) Power per unit frequency emitted by the oscillator, consisting of discrete modes labeled by the index m. In reality, the modes have a finite width. (b) Transmission vs frequency for light incident at 0 deg to the filter FP mirrors. The transmission peak frequencies do not necessarily coincide with peaks in the oscillator output spectrum. (c) Transmission vs frequency for a nonzero incidence angle θ.
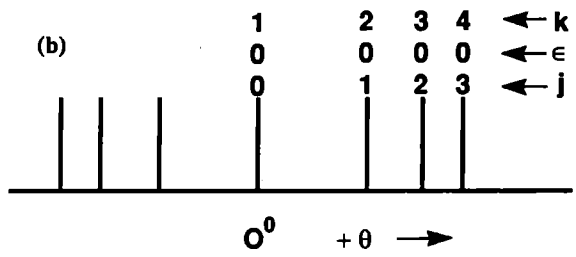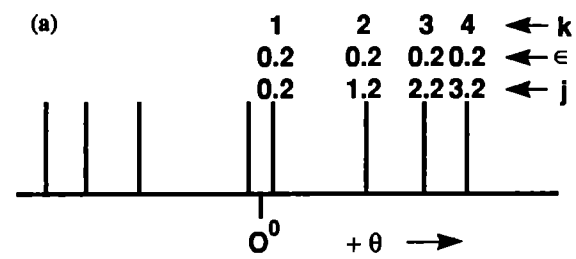
Figure 7. (a) Power per unit frequency for the oscillator output in the continuum model assumed. (b) Power per unit solid angle assumed for the angular distribution of light exiting the telescope, normalized to unity power.
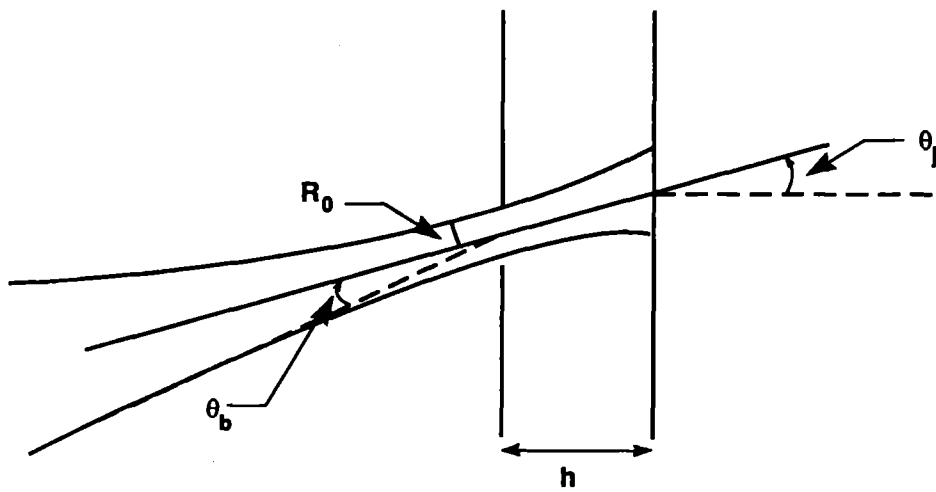
Top view

Side view
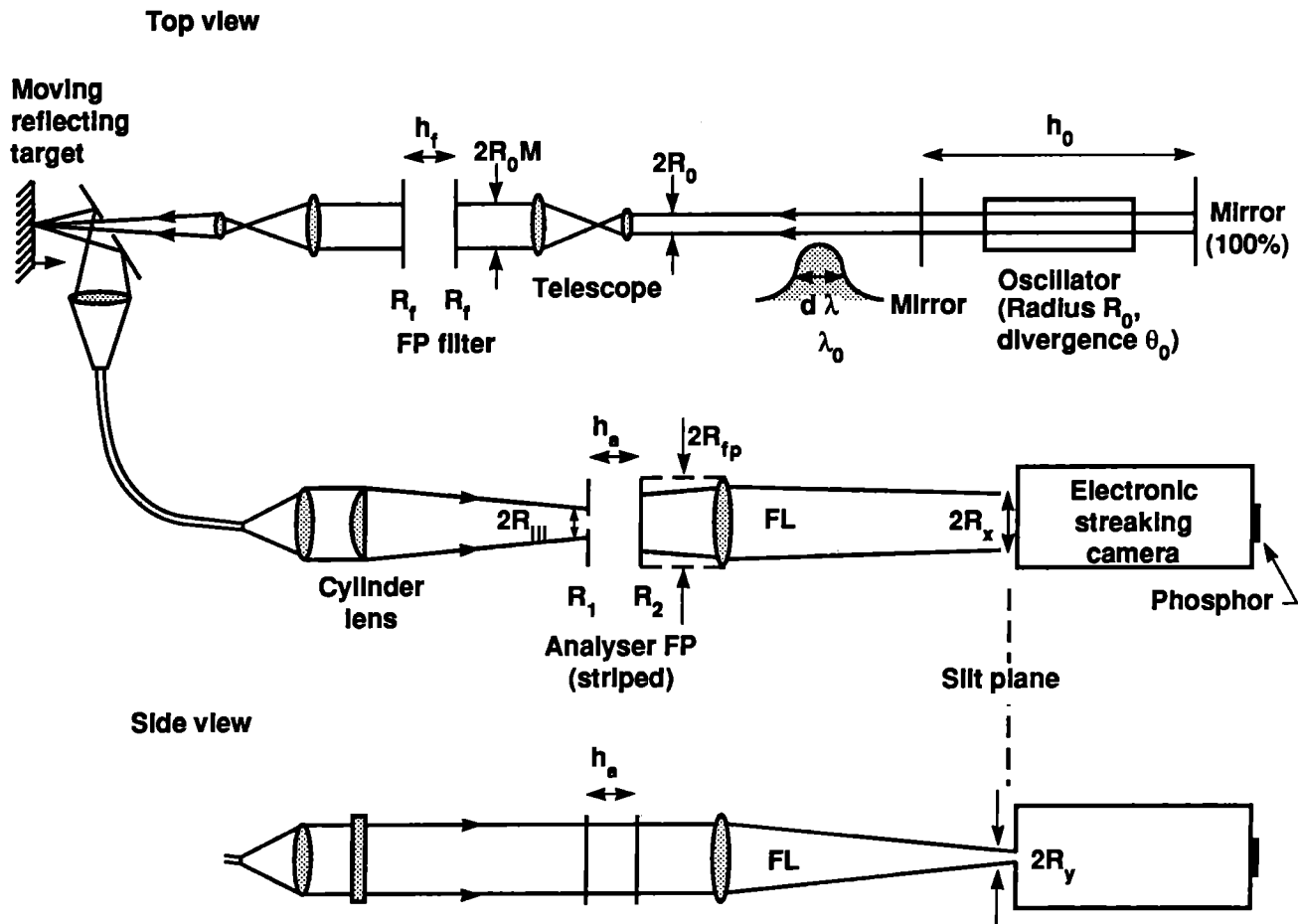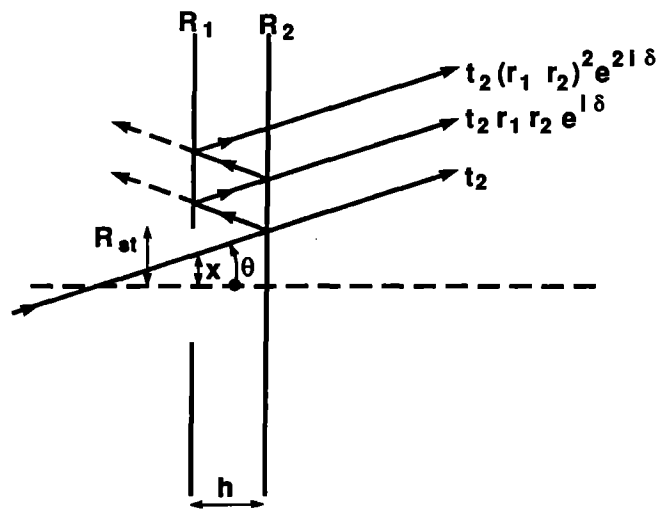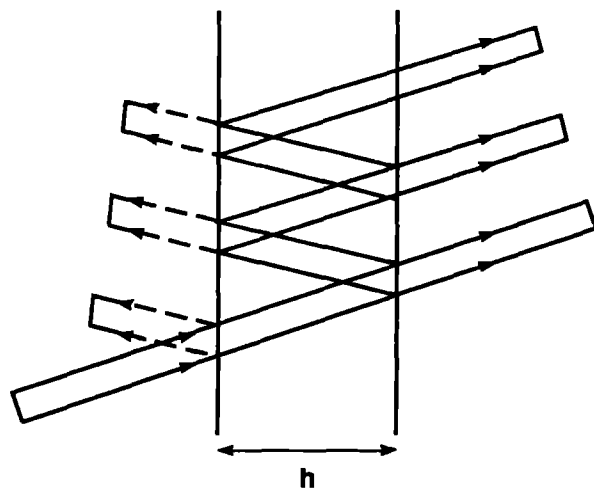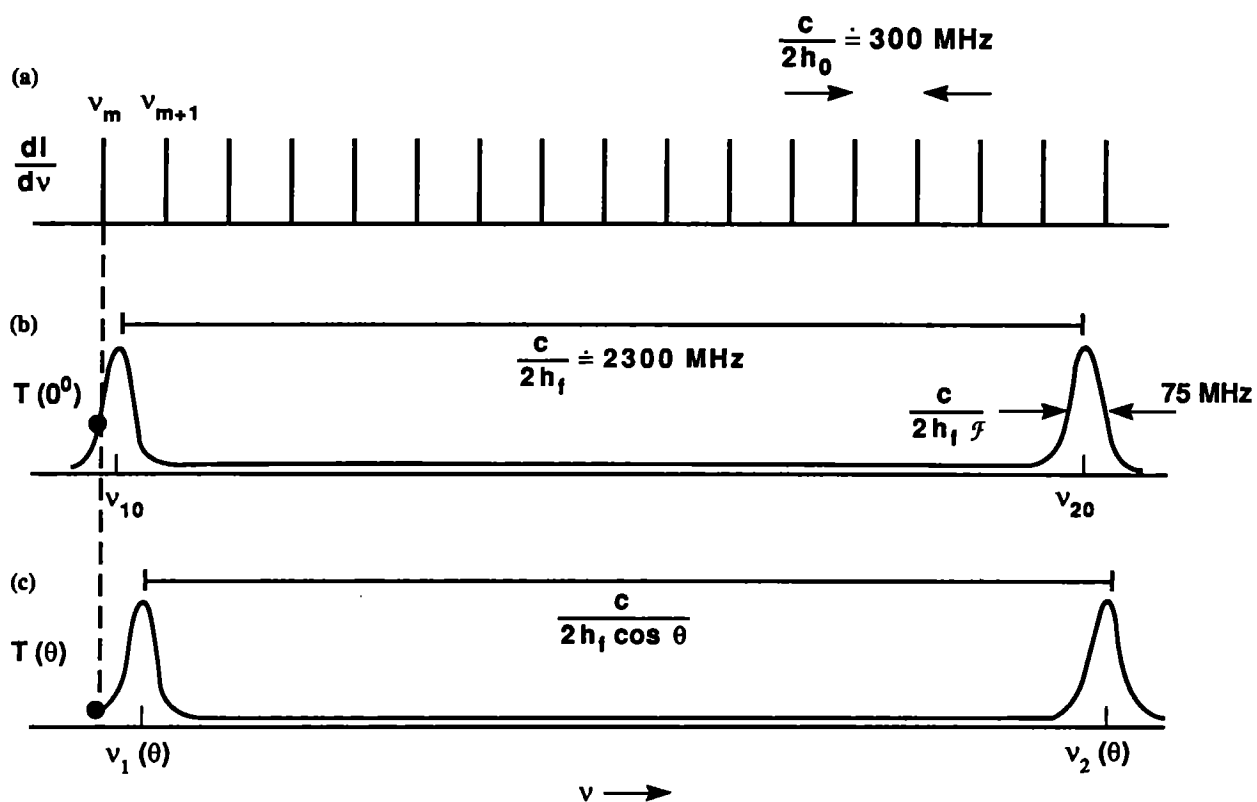

D. R. GOOSMAN - Fig. 1

D. R. GOOSMAN - Fig. 2

D. R. GOOSMAN - Fig. 3

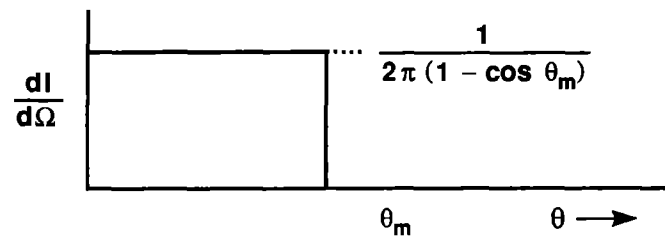D. R. GOOSMAN - Fig. 4

h

D. R. GOOSMAN - Fig. 5

$\frac{c}{2h_0} \doteq 300$ MHz

(a)

ν_m ν_{m+1}

$\frac{dI}{d\nu}$

(b)

$T(0^0)$

$\frac{c}{2h_f} \doteq 2300$ MHz

$\frac{c}{2h_f \mathcal{F}}$

75 MHz

ν_{10}

ν_{20}

(c)

$T(\theta)$

$\frac{c}{2h_f \cos\theta}$

$\nu_1(\theta)$

$\nu_2(\theta)$

$\nu \longrightarrow$

D. R. GOOSMAN - Fig. 6

31
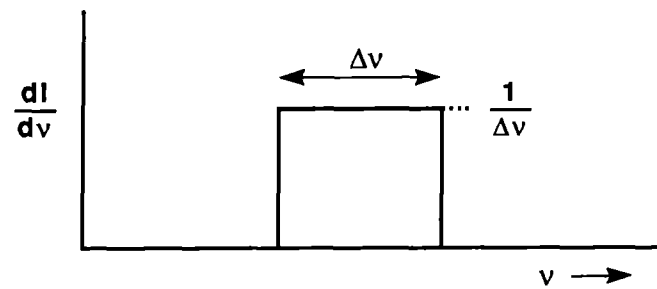
D. R. GOOSMAN - Fig. 7

Table I. Fringe number, combined finesse due to reflectivity and walkoff, and estimate from Eq. (54) for R = 0.97 and R_{fp} = 2.5 cm. The reflectivity finesse is 101.5.

	h_a = 6.5 cm			h_a = 15 cm	
Fringe #	$\mathscr{F}_{arw}$	Eq. (54)	Fringe #	$\mathscr{F}_{arw}$	Eq. (54)
1	73.0	73.6	1	58.7	59.8
2	46.2	46.8	2	32.9	33.1
3	36.2	36.3	3	24.5	24.1

Appendix 1: Stripe Region Without an Antireflection Coating

If the region within the stripe does not have an antireflection coating, then another treatment of the transmission pattern is necessary. Figure A-1 shows three regions of different reflectivities, with the stripe region being characterized by the zero subscripts. Without an antireflection coating, rays may reflect with about 4% intensity from surface 0, the stripe region. We would expect this to cause a weak component of light with broader fringes to add to the usual pattern, but with no shift in peak angle, provided surfaces 0 and 1 are equidistant from surface 2.

The latter provision is usually not true, however. A further complication arises because the coating on mirror 1 has finite thickness. We assume that that coating is evaporated over a perfectly flat surface. Then the phase shift δ_2 due to reflection from surfaces 2 and 0 in succession is different from the phase shift δ resulting from successive reflections from surfaces 2 and 1. This is expected to produce a slight shift in peak position, because not all of the beamlets are in phase.

The number N of beamlets exiting mirror 2 is given by Eq. (53) and is limited by the radius of the mirrors.

We assume that the value of p_{str} = 3.99 in Eq. (24) determines R_{st}. This means that there will be either zero or one reflection from the coating within the stripe. We denote by A_1 and I_1 the amplitude and transmission, respectively, due to an incident ray that never reflects from surface 0, and let A_2 and I_2 apply for a ray that reflects exactly once from this region. Then I_1 is easily shown to be simply T_0 times the right-hand side of Eq. (52) with $h\theta = R_{st}$. The amplitude A_2 is

$$A_2 = t_0 t_2 \left\{ 1 + r_2 r_0 e^{i\delta_2} \left[1 + r_1 r_2 e^{i\delta} + \cdots + \left(r_1 r_2 e^{i\delta} \right)^{N-2} \right] \right\} . \tag{A1}$$

This amplitude can be summed and squared to give

$$I_0 = \frac{T_0 T_2}{1 + R^2 - 2R\cos\delta} \left\{ 1 + R^2 + R_3^2 (1 + R^{2N-2}) - 2R\cos\delta + 2R_3\cos\delta_2 \right.$$

$$- 2RR_3\cos(\delta - \delta_2) - 2R_3 R^{N-1}\cos[\delta_2 + \delta(N-1)]$$

$$\left. + 2R_3 R^N \cos[\delta_2 + \delta(N-2)] - 2R_3^2 R^{N-1}\cos[\delta(N-1)] \right\} , \tag{A2}$$

where R, T_2, and δ are defined by Eqs. (4), (5), and (2) respectively, and

$$R_3 = r_2 r_0 \quad \text{and} \quad T_0 = 1 - R_0 . \tag{A3}$$

In order to see the effect of the finite coating thickness and finite value of R_0, we assume that the mirrors are large enough to allow the complete pattern to form. Then I_1 reduces to Eq. (3) and I_2 becomes

$$I_2 = \frac{T_2 T_0}{1 + R^2 - 2R\cos\delta} \left[1 + R^2 + R_3^2 - 2R\cos\delta + 2R_3\cos\delta_2 - 2RR_3\cos(\delta - \delta_2) \right] . \tag{A4}$$

We further simplify by assuming that $R_1 = 1$ and that we have spatially incoherent illumination forming a waist at the stripe, with no correlation between angle and position. Then we can write

$$I = q I_1 + (1 - q) I_2 . \tag{A5}$$

Substituting the above results and rearranging gives

$$I = \frac{T_0 T_2}{1 + R^2 - 2R\cos\delta} \left(q + (1 - q) \left\{ 1 + R^2(1 + R_0) \right. \right.$$

$$\left. \left. + 2R \left[\sqrt{R_0} \cos(\delta + \phi) - R\sqrt{R_0}\cos\phi - \cos\delta \right] \right\} \right) , \tag{A6}$$

where q is defined by Eq. (20), the reflectivities and transmissivities are defined by Fig. A-1, and the phase difference ϕ is

$$\phi = \frac{4\pi\Delta h \cos\theta}{\lambda} \quad , \tag{A7}$$

where Δh is the effective optical thickness of the coating on surface 1, which we treat as an unknown.

We have evaluated Eq. (A6) numerically, allowing the unknown phase to take on any value from 0 to 360 deg. A test was made to see if the peak transmission angles for any ϕ shifted from the values obtained by setting $\phi = 0$. For h = 6.5 cm and also 2 cm, and R = 0.97 with R_0 = 0.04, we could not produce a peak angle shift larger than 0.01% for any value of ϕ.
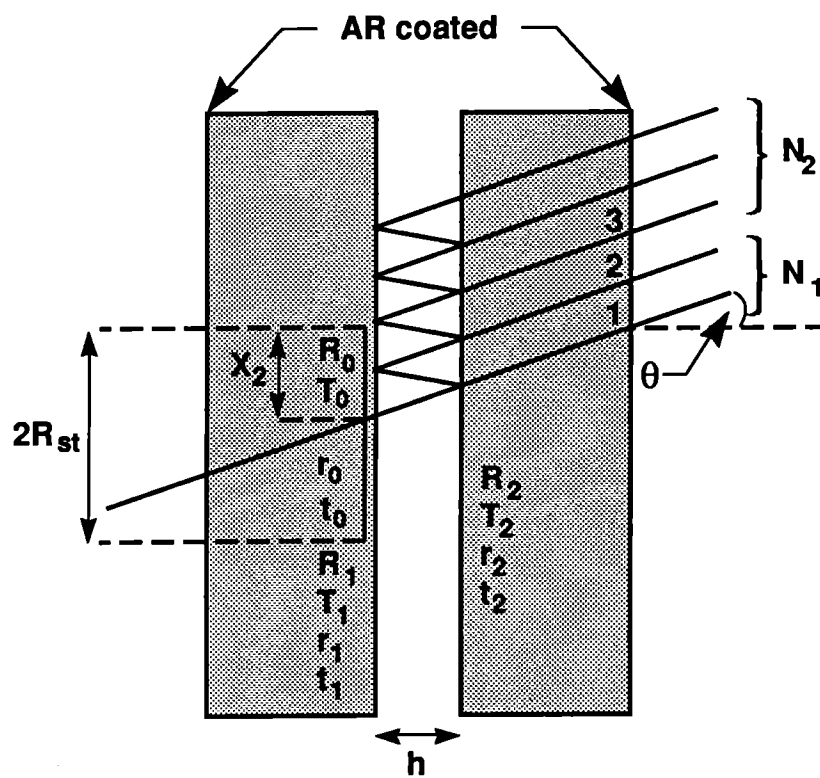
The second test was an analytical comparison for $\phi = 0$ of patterns for R_0 = 0.04 with those for R_0 = 0. It is easy to show that for $\phi = 0$, the term in Eq. (A6) multiplying $(1 - q)$ is simply the reciprocal of the normal FP pattern for an effective reflectivity

$$R_4 = \sqrt{R_2}(1 - R_0) = R\sqrt{1 - R_0} \quad . \tag{A8}$$

Then the complete pattern, I, has slightly broader fringes for R_0 = 0.04 than for R_0 = 0, but with the same peak angles.

We summarize the situation for spatially incoherent illumination whose waist is at the stripe of an FP with very large mirrors with $R_1 = 1$ and $R_{st} = \sqrt{3.99\,\lambda\,h}$. Reflections from an uncoated interface with R_0 = 0.04 produce a negligible peak angle shift for normal circumstances, even for finite coating thicknesses.

Figure A-1. Beamlets formed in an FP, where we assume that the striped region has nonzero reflectivity R_0. The rest of the mirrors are denoted by reflectivity and transmission coefficients with subscripts 1 and 2, respectively. The first N_1 beams (to within 1) have not reflected from the coating with reflectivity R_1. The remaining N_2 beams have reflected from R_1. N_2 is finite due to the finite size of the FP mirrors.

AR coated

N_2

N_1

θ

X_2

R_0
T_0

$2R_{st}$

r_0
t_0

R_2
T_2
r_2
t_2

R_1
T_1
r_1
t_1

h

D. R. GOOSMAN - Fig. A-1